Article

Synergistic Inhibition Guided Fragment-Linking Strategy and Quantitative Structure−Property Relationship Modeling To Design Inhalable Therapeutics for Asthma Targeting CSF1R

Tasneem M. Vaid, Robel Demissie, Youngjin Kwon, Thao Tran, Hyung-Geun Moon, José A. Villegas, Gye Young Park, Michael E. Johnson,* and Hyun Lee*

Read Online

ACCESS | Metrics & More | Article Recommendations | SI Supporting Information

ABSTRACT: The colony-stimulating factor-1 receptor (CSF1R) is a tyrosine-protein kinase that is a potential target for asthma therapeutics. We have applied a fragment-lead combination approach to identify small fragments that act synergistically with GW2580, a known inhibitor of CSF1R. Two fragment libraries were screened in combination with GW2580 by surface plasmon resonance (SPR). Binding affinity measurements confirmed that thirteen fragments bind specifically to the CSF1R, and a kinase activity assay further validated the inhibitory effect of these fragments. Several fragment compounds enhanced the inhibitory activity of the lead inhibitor. Computational solvent mapping, molecular docking, and modeling studies suggest that some of these fragments bind adjacent to the binding site of the lead inhibitor and further stabilize the inhibitor-bound state. Modeling results guided the computational fragment-linking approach to design potential next-generation compounds. The inhalability of these proposed compounds was predicted using quantitative structure−property relationships (QSPR) modeling based on an analysis of 71 drugs currently on the market. This work provides new insights into the development of inhalable small molecule therapeutics for asthma.
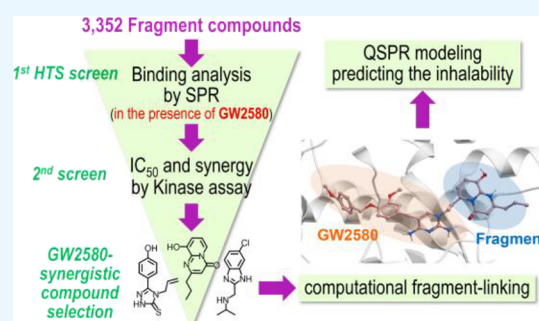
INTRODUCTION

Asthma is a chronic respiratory disease with intermittent flare-ups. The primary event leading to the progression of asthmatic symptoms in individuals is allergen sensitization, whereupon repeated exposure to allergens (e.g., pollens, ragweed etc.,), an individual becomes sensitized by developing specific antibodies. Once sensitized, individuals develop inflammation in the lung airways, resulting in the shortness of breath upon re-exposure to the sensitized allergen(s). Despite the current medical treatment using the conventional asthma therapy consisting of inhaled corticosteroids,[1] inhaled corticosteroids plus long-acting β-agonist combination,[2] and/or bronchodilators, many asthma patients still develop chronic refractory asthma with long-term disability. Since the last decade, there have been no novel asthma therapeutics introduced except for antibody-based biologic agents, the safety profile and long-term effects of which are yet to be established.[3]

During sensitization, dendritic cells (DCs) in the airway capture and process the invading allergen and migrate to regional lymph nodes to activate the adaptive T helper type 2 (Th2) immune response, resulting in the establishment of allergen-specific memory and exacerbation of the existing allergic inflammation. Suppressing the initial sensitization process could therefore preclude the subsequent events of the Th2 allergic inflammatory process, which will be ideal for asthma maintenance therapy. Conventional therapies do not deal with the initial allergen sensitization but rather block the subsequent events such as T-cell activation, eosinophil recruitment, and bronchoconstriction.

Colony-stimulating factor-1 receptor (CSF1R), a transmembrane receptor tyrosine kinase, is expressed mainly in mononuclear phagocytes, e.g., DCs, monocytes, and macrophages. Mammalian CSF1R is found exclusively at the surface of mononuclear phagocytes and their progenitors[4] and is known to regulate the survival, proliferation, differentiation, and chemotaxis of tissue macrophages and DCs that play key roles in innate immune responses.[5] CSF1R and its ligand, colony-stimulating factor-1 (CSF1), regulate the functions of DCs in allergen sensitization. In allergen-stimulated inflammation, airway epithelial cells primarily secrete CSF1, which binds to its cognate receptor CSF1R and triggers its dimerization, followed by the auto-phosphorylation of the kinase domain
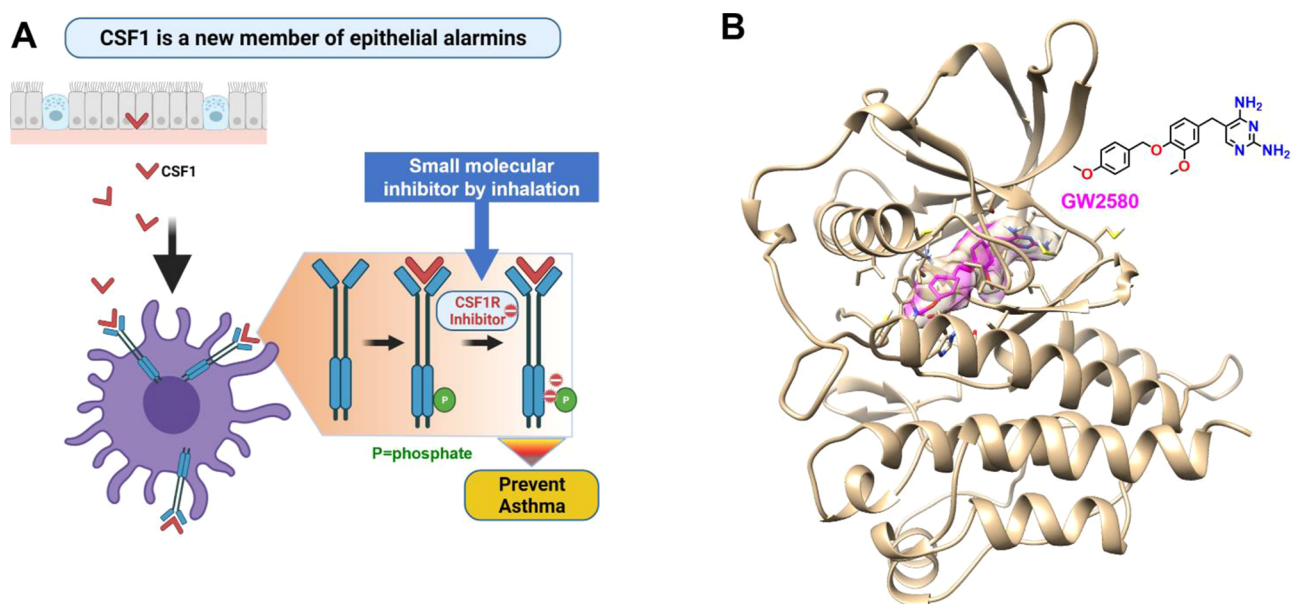
Figure 1. (A) Potential mechanism of action of small molecule inhibitors against CSF1R. (B) Structure of CSF1R bound with GW2580 (pink).
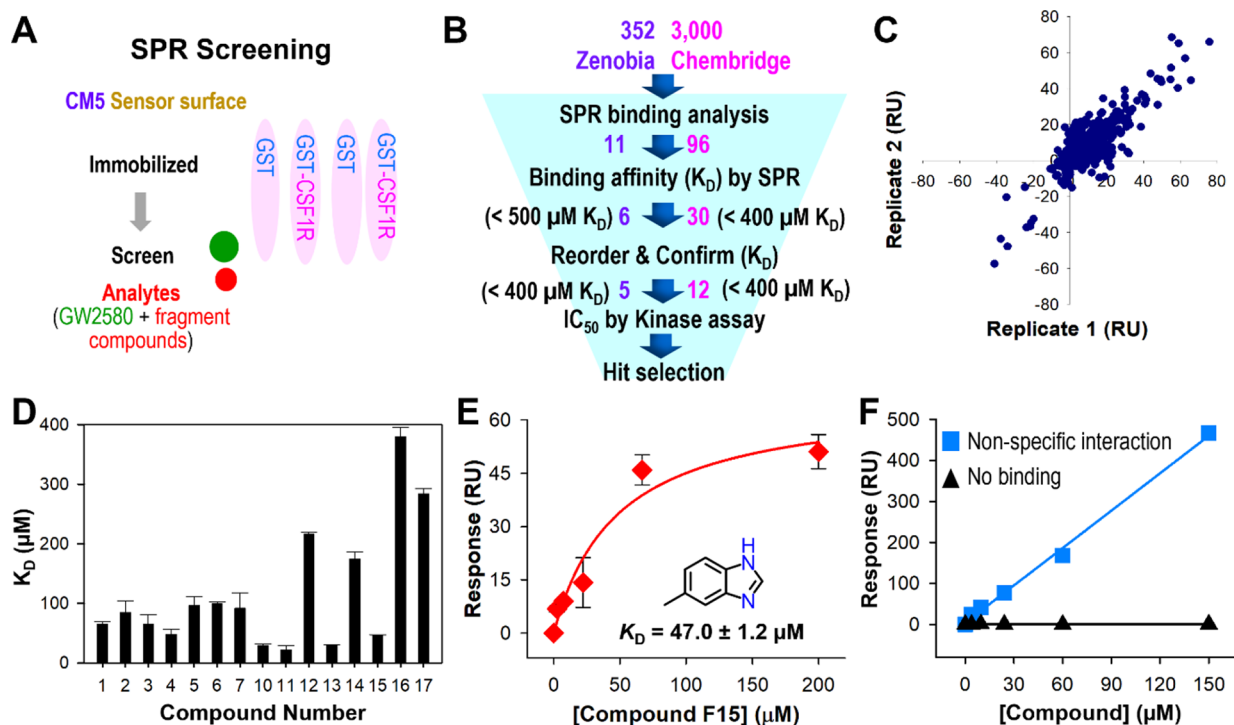

Figure 2. Fragment screening and hit validation. (A) SPR screening strategy. To screen small fragment molecules having synergy with GW2850 when both bind to CSF1R, we adopted the strategy outlined here. A bound complex of CSF1R and GW2850 serves as the target for additional binding of fragment molecules. Binding of the fragment (red) in the presence of GW2580 (green) will provide an enhanced binding signal. (B) 3352 fragments from two different fragment libraries were screened by SPR with immobilized GST-tagged CSF1R. One hundred and seven fragments were cherry-picked and binding affinities (K_D) were determined. Among them, 36 fragments showed K_D values lower than 500 μM. (C) Replicate plot of 3352 fragments in duplicates. (D) K_D value determination. Through the process of validating K_D values, 17 fragments were confirmed to have binding affinities below 400 μM. (E) Binding curve for compound F15 (ZT0020). (F) Binding curves showing nonspecific interaction and no binding.

which further activates multiple downstream pathways. Recently, we found that the binding of CSF1 to CSF1R results in the trafficking of DCs to the regional lymph node, which in turn facilitates the process of allergen sensitization.[6] Hence, blocking CSF1 binding to CSF1R could potentially inhibit the primary process of allergen sensitization.

Although multiple CSF1R inhibitors are in various stages of clinical development,[7] we have chosen GW2580, which exhibits low nM binding affinity to CSF1R, for our starting scaffold due to its high inhibitory efficacy and high kinase selectivity[8] for further development. The potential mechanism of action of small molecules inhibiting CSF1R and the crystal
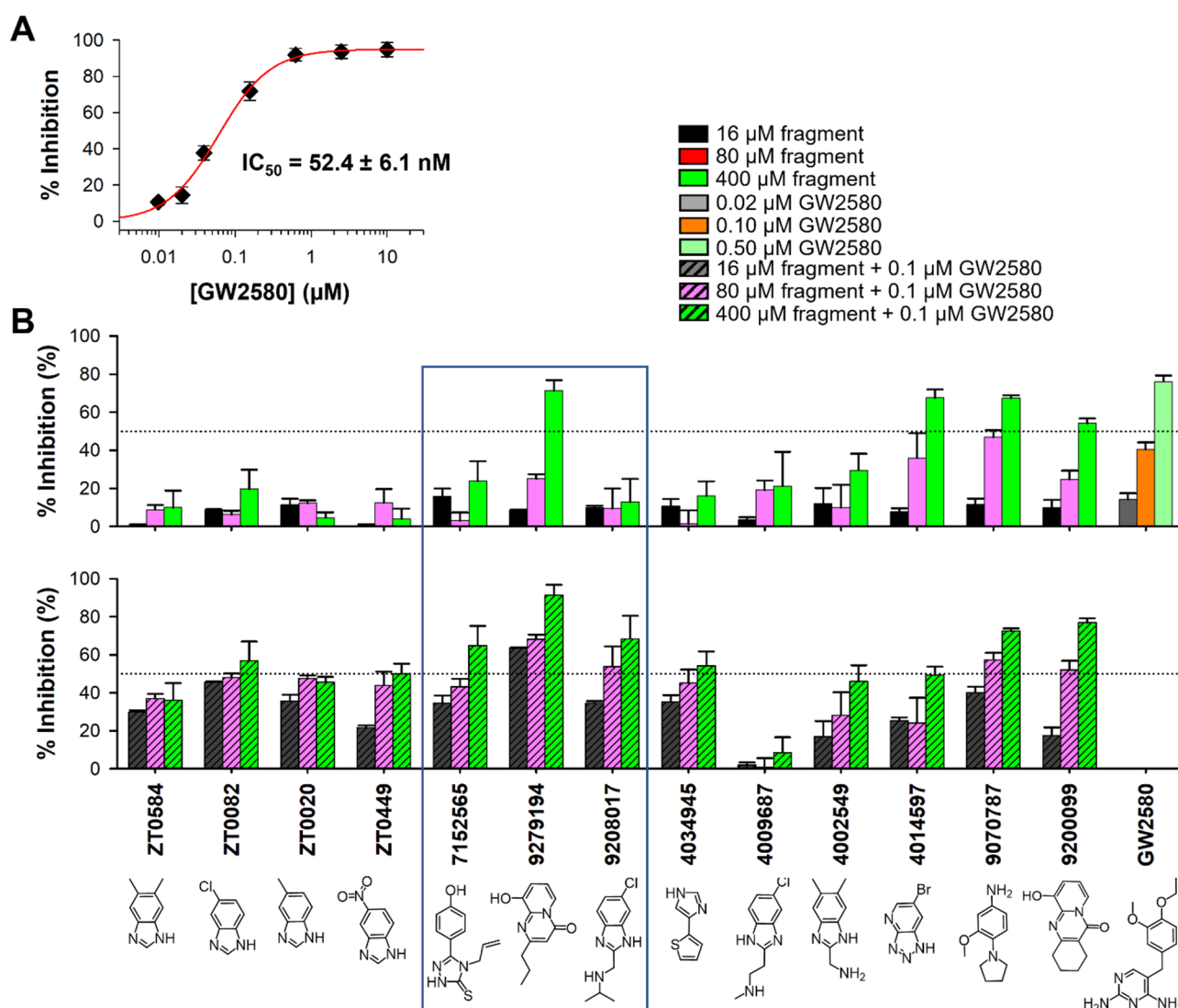
Figure 3. CSF1R kinase activity. (A) Dose−response curve of GW2580 to measure half-maximal inhibitory concentration (IC_{50}). The determined IC_{50} value was 52.4 ± 6.1 nM. (B) Percent inhibition of individual fragment compounds and GW2580 at three different concentrations (upper panel) and in the presence of 0.1 μM GW2580 (lower panel).

structure of GW2580 bound CSF1R[9] are shown in Figure 1. Work using nanoparticles carrying GW2850 showed therapeutic potential for asthma by intranasal delivery.[10] However, GW2580, originally developed by GlaxoSmithKline (now GSK) as a tool compound,[10] is not ideal for asthma therapy, as it has high systemic bioavailability.[11−13] In fact, all currently available CSF1R inhibitors appear to have been designed exclusively for systemic delivery to treat malignant diseases. Systemic exposure produces a wide variety of physiological consequences. To minimize adverse systemic reactions and maximize therapeutic effect in airways, an inhalational agent is preferred for asthma therapy.

Computer-aided drug design using molecular modeling, including molecular dynamics simulations and molecular docking, has been widely used as a powerful technology in the drug discovery pipeline.[14−16] Recently, machine learning methodologies have taken an emerging role in drug discovery, ranging from molecular/material property prediction to synthesis planning.[17] Our fragment linking strategy was guided by molecular dynamics simulations and docking calculations, followed by prediction of inhalability using a QSPR

classification model that was generated based on 71 currently marketed drugs. In general, inhalational drugs are known to have somewhat higher molecular weights and more polar structures.[18−20]

In this study, we aim at developing a novel inhalable small molecule compound that inhibits allergen sensitization, targeting the initial events by inhibiting CSF1R. We have utilized the strategy we developed previously[21,22] to screen for small fragment molecules that bind synergistically with GW2850 to CSF1R. For one such synergistic fragment, 9279194, we have outlined a fragment-linking strategy, guided by computational calculations, to efficiently couple its multiple analogs to GW2580. A series of fragment-linked potential inhibitor compounds have been proposed with characteristics more aligned with inhalational administration, as predicted by our QSPR model.

■ RESULTS AND DISCUSSION

Fragment Screening and Binding Analysis Using SPR. Binding affinities of many fragment compounds are typically very weak, and hence, surface plasmon resonance (SPR) was

used to detect direct binding to the GST-tagged CSF1R, as it is very sensitive and can detect weak binding up to 2−5 mM binding affinity, depending on the solubility. We screened 3352 fragments from two different fragment libraries: (I) Zenobia library of 352 compounds[23] and (II) 3000 fragments from the Chembridge fragment collection of 10,000,[24] in turn selected from the ZINC database[25] of more than 10 million. These fragments were selected for chemical properties compatible with GW2580 modification. The GST-linked CSF1R protein was immobilized on a CM5 sensor chip and fragments were screened in the presence of GW2580 (Figure 2A) in duplicate. Duplicate results agreed well as can be seen in the replicate plot (Figure 2C). Fragments (107) were cherry-picked, and binding affinities (K_D) were determined, 36 of which showed K_D values lower than 500 μM. Thirty-six repurchased fragments were re-evaluated for K_D values, and 17 were confirmed to have binding affinities below 400 μM, seven of which exhibited K_D values lower than 100 μM (Figure 2D). The steady-state affinity fitting curve of fragment 15 (F15) is shown as an example (Figure 2E) along with nonspecific binders and no binding curves (Figure 2F). Thirteen fragments were chosen for further validation by enzymatic activity assay.

Determination of Inhibitory Activity and Synergy Using In Vitro Kinase Assays. The in vitro kinase assay was optimized using a commercially available ADP-Glo Kinase Assay kit, and inhibitory activity (IC_{50}) of GW2580 was determined to assess our kinase assay as a control. The IC_{50} of GW2580 was determined to be 52.4 nM, which is comparable to reported values. Thirteen selected fragments, four from Zenobia and nine from the Chembridge library, were tested in the absence and presence of 0.1 μM GW2580 at three concentrations (16, 80, and 400 μM). Most of the fragments showed an additive effect on CSF1R kinase inhibitory activity, while three fragments (7152565, 9279194, and 9208017) showed a slightly more additive effect, suggesting potential synergy (Figure 3). Full dose−response of these three selected fragments in combination with GW2580 were investigated, two of which (7152565 and 9279194) displayed ∼2-fold enhanced IC_{50} values (Figure 4).
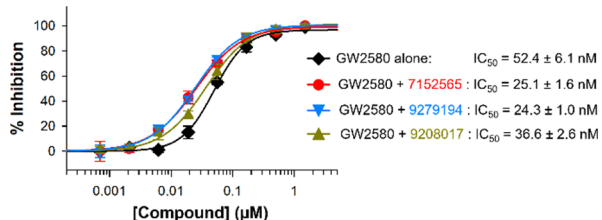

Figure 4. Enhancement of inhibitory activity. Dose−response curve of GW2580 alone and in combination with each of three selected fragments, 7152565, 9279194, and 9208017.

Binding Hotspot Analysis Using FTMap and ICM-PocketFinder. Our binding synergy analyses using SPR suggest that these newly identified fragment-like compounds bind to a site separate from that of the lead inhibitor, GW2580. Therefore, all possible binding site candidates were investigated. A series of computational solvent mapping calculations, or "hotspot" analyses, were performed using the FTMap[26] server. FTMap is a multistage protein mapping algorithm that is based on a fast Fourier transform (FFT) correlation. This approach can efficiently search for potential binding sites on the entire surface of the protein.

A crystal structure of GW2580 bound CSF1R kinase[9] was used for the analyses. The crystal structure indicates that there are a few crucial interactions governing ligand stabilization, including a $\pi-\pi$ interaction with W550; π−cation interactions with Y665; and hydrogen bonding interactions with the backbone of D796, E664, and C666, as shown in the ligand interaction plots in Figure S5A. A short molecular dynamics (MD) simulation was carried out to refine the protein−ligand complex structure before docking and to sample the side-chain conformations of protein residues. The RMSD analyses indicated the stable protein-ligand conformation, with RMSD <2 Å for both the protein backbone and ligand (Figure S5B), indicating the absence of any major conformational fluctuations.

Next, the cluster-representative frames (15 in total) were extracted from the simulations as discussed (see Methods in Supporitng Information file) and submitted to the FTMap server, which performed a fragment-based binding site analysis. One strong fragment binding site was identified by analyzing the cluster of representative structures and consensus clusters of the probe molecules. The hot spot identified by this analysis appears to be an extension of the original binding site of the lead inhibitor GW2580 (Figure 5). This pocket has been
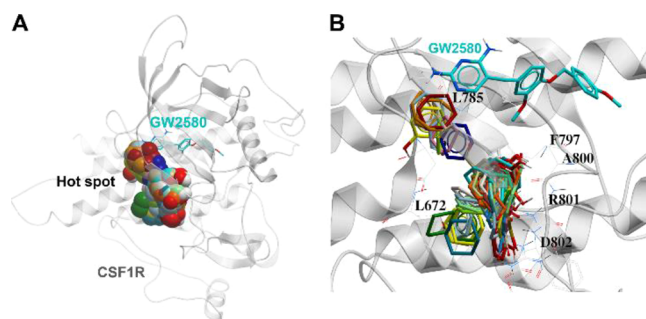

Figure 5. Binding hotspot analysis. The hot spot identified by FTMap server is shown along with the GW2580 bound to the crystal structure of CSF1R kinase (shown in ribbon). The GW2580 is shown in a stick representation (cyan). (A) The hot spot is depicted by a superimposition of the various probes shown in the CPK representation. The carbon atoms from the probes are colored differently based on their binding to a specific cluster representative structure. (B) A close-up view of the binding pocket shows four major probes (benzene, benzaldehyde, phenol, and cyclohexane) in stick representation, showing the presence of the binding hot spot. Same probe from different structures is colored differently. Some of the binding pocket residues in CSF1R are labeled and shown in stick representation.

partially explored in the inhibitor bound DFG-out conformation of CSF1R crystal structures (PDB ID: 3LCO and 6IG8). This extended cavity is composed of five residues: G46, A47, F193, A196, R197, and D198.

The ICMPocketFinder function[27,28] was also used as an orthogonal tool to identify the putative fragment binding pockets. For the GW2580-bound CSF1R kinase structure,[9] the tool predicted five pockets (Figure S3A). Factors that can influence ligand binding to a pocket include the pocket volume and surface area, buriedness, hydrophobicity, and how compact the pocket is. All of these properties calculated using ICMPocketFinder are tabulated (Figure S3B). Pocket no. 2 (highlighted in bold in Figure S3B) is the same pocket identified by FTMap, as shown in Figure S3A (in red).

Fragment Binding Site Analysis. To further investigate the fragment binding site and to predict the most likely binding conformation of the fragments, we performed a series of computational calculations. These studies, described in detail in the Methods section of the Supporting Information file, used a combination of molecular docking and molecular simulations. To screen the potential hotspot binding fragments, first, the docking was performed on the apo-receptor spanning the full receptor surface. All 17 SPR hits which showed binding affinities below 400 μM in SPR were docked individually. Rigid docking, which does not account for receptor or ligand flexibility, and flexible docking, which accounts for only fragment flexibility, were employed. Both rigid and flexible docking indicated that all fragments show binding to the hotspot identified by FTMap and ICM PocketFinder methods.

Next, flexible docking was performed on CSF1R kinase bound to GW2580, focusing on the three fragments (7152565, 9279194, and 9208017) that showed synergy with GW2580 in the kinase assays. As discussed above, structural analyses and computational solvent mapping of the co-crystal structure of GW2580 bound CSF1R kinase, identified one "hotspot", i.e., a potential fragment binding site, located adjacent to the pyrimidine group of GW2580. The binding pocket area for docking was defined to be within 12 Å from the GW2580 binding pocket. Docking was performed against all of the 15 cluster-representative structures extracted from the MD simulation trajectory. The docked conformations of the fragments were scored and ranked by the "Grid Score" scoring function. In total, 20 conformers were scored for each fragment, which were clustered by 2 Å RMSD. Five top-scoring conformers were selected based on (I) binding within "linkable" distance, i.e., within 2.5 Å from the pyrimidine group of the bound GW2580 and (II) the cluster size.

Based on the grid score, the top five conformers of the three fragments were subjected to more rigorous secondary screening using Amber score, which takes into account both receptor and ligand flexibility. For fragment 7152565, three conformers scored well (< -20), but the docked Amber scored conformation showed that the fragment is binding more than 4 Å away from the GW2580 pyrimidine group. Linking such a fragment would result in a compound with a higher molecular weight, not in the acceptable range for a small molecule drug. For fragment 9279194, two conformers scored well (< -20). Their docked conformations are also linkable. For fragment 9208017 conformers, the scores are very high. Hence, two conformers of 9279194 were explored for the next, fragment-linking strategy. Table 1 lists the docking scores (grid scores and Amber scores) generated by Dock6.9,[29] of the fragments when docked to the GW2580-bound CSF1R kinase MD
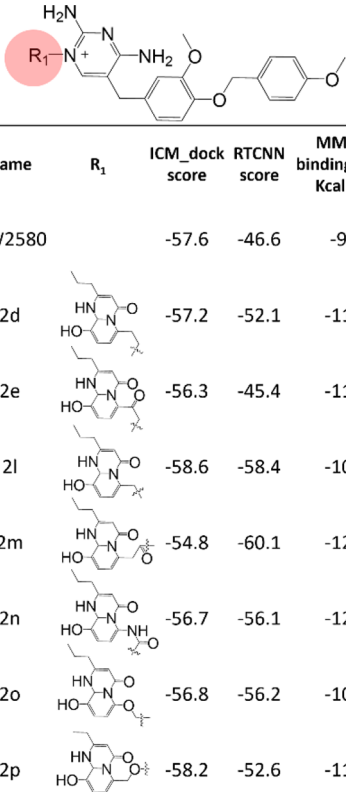
frames. The scores are shown for the top five conformers of fragments 7152565, 9279194, and 9208017.

To prioritize compound candidates for future synthesis and testing, a series of fragment linking and docking analyses was performed, using the information determined from the binding site prediction studies discussed above. A variety of linked fragments were generated (Figure S4) based on the two lowest energy conformers of 9279194. Broadly two types of linkages were tested: (1) 9279194 linked to the meta-nitrogen of the pyrimidine group in GW2580; (2) 9279194 linked to the para-amine of the pyrimidine group in GW2580. Proposed linked compounds are selected based on their docking scores and their ability to successfully recapitulate the key binding features of the inhibitor (as shown in the ligand interaction plots in Figure S5A) and the synergistic fragment. With the two types of fragment-linked compounds, only the fragments linked to the meta-nitrogen of the pyrimidine group of GW2580 retained the bound conformation of the unlinked GW2580/ fragments (as shown in Figures S6 and S7).

The structures of these fragment-linked compounds along with the docking scores and MM/GBSA binding energy values are shown in Figure 6. Two different docking scores are reported: (1) ICM_dock score, a MM/GBSA-type scoring function generated by ICM. (2) RTCNN Score, a neural network Score, which does not use any molecular mechanics or

Name	R$_1$	ICM_dock score	RTCNN score	MMGBSA binding energy Kcal mol^{-1}	Route of administration by ANN model
GW2580		-57.6	-46.6	-96.5	**oral (97%)**
2d		-57.2	-52.1	-116.9	**inhalational (92%)**
2e		-56.3	-45.4	-115.1	**inhalational (92%)**
2l		-58.6	-58.4	-109.8	inhalational (78%)
2m		-54.8	-60.1	-122.3	**inhalational (92%)**
2n		-56.7	-56.1	-120.1	inhalational (78%)
2o		-56.8	-56.2	-109.5	inhalational (78%)
2p		-58.2	-52.6	-117.4	inhalational (78%)

Figure 6. Fragment-linked analogs of GW2580. A table showing the structures, docking scores, MM/GBSA binding energy values and inhalability predictions of the linked analogs (the percent confidence estimates are listed in brackets. The high-confidence predictions are highlighted in bold). The first row shows values for GW2580 for comparison. The GW2580 structure is shown on the top. R1 represents the corresponding R1 group in reference to the top structure.

Table 1. Docking Scores by Dock6.9[29]

fragment	grid scores	Amber scores[a]
7152565	−30.6, −30.2, −27.5, −28.4, −30.2	−20.5, −23.4, −27.9, 23.7, −7.8
9279194	−25.1, −25.0, −25.9, −25.4, −24.3	−31.6[a], −24.6[a], 28.6, 22.4, −10.7
9208017	−29.2, −30.3, −28.8, −27.4, −29.0	11.3, −0.9, 0.9, −12.6, 3.2

[a]Amber scores for the two conformers of 9279194, which showed lower scores and the linkable conformation.

physical energy terms. Instead, the score is trained to recognize native-like complexes versus decoys directly, based only on geometries of putative complexes. ICM_dock scores for all linked compounds are comparable to GW2580 (-57.6 ± 3). The RTCNN scores show more variations with most of the compounds being lower than GW2580 and 2 m showing the lowest scores. For MM/GBSA energy values, all linked compounds exhibit values lower than GW2580, indicative of enhanced binding, with 2 m possessing the lowest binding free energy.

ANN Model To Predict the Route of Administration for the Linked Compounds. In total, 226 descriptors (inputs) were calculated by the ADMET predictor. Zero inputs had a CV% of less than 1%. Twenty-six inputs are under-represented, i.e., the nonzero values were less than 4. Twenty-seven pairs of inputs were highly correlated, and 105 inputs were found to be highly correlated with others. After removing low CV, underrepresented, and highly correlated variables, the final maximum number of descriptors that were used to build the model was 68. For our classification model, the best model (highlighted in green in the model grid shown in Figure S2) was obtained with 1 neuron and 11 inputs (descriptors). The top ranked 11 descriptors are listed in Table S2 along with their sensitivities, relative sensitivities, and explanations of the descriptor codes. The descriptor sensitivity rankings are the same for all architectures in the model grid.

The performance statistics are shown in Figure 7. For the training set, sensitivity was 1, specificity was 0.974, MCC was 0.959, and the false rate was 0.018. For the test set, the sensitivity was 1, specificity was 0.833, MCC was 0.866, and the false rate was calculated to be 0.067. The confidence analysis generated a Min confidence value of 0.47, which is in the acceptable range of 0.5 ± 0.05.[30] To verify that the model was not constructed by an accidental correlation between the dependent variables and the descriptors, the values of the dependent variable were shuffled at random. The MCC values for none of the generated ensembles were more than 0.5 for both the training and the test set, which verifies the true correlation between the dependent variable and the descriptors.

Based on the prediction of inhalability by the generated ANN model, three analogs (2d, 2e, and 2m) are predicted with the highest confidence to have properties more aligned with inhalational administration (Figure 6, column 6).

CONCLUSIONS

In attempts to develop a high potency CSF1R inhibitor, two fragment-like libraries were screened in combination with a lead inhibitor, GW2580, by direct binding analysis using SPR. Initial hits (107) were further narrowed down to seventeen fragments by determining their binding affinities (K_D). Kinase inhibitory assays validated the synergistic or additive effect of these fragment binders. We discovered a total of three fragment-like compounds that synergistically enhanced the inhibitory activity of lead inhibitors. Computational analysis predicted a "hotspot" that could be a potential fragment binding site, which is an extension of the lead inhibitor binding site. Enzymatic characterization and computational studies suggest that these fragments, by binding adjacent to the binding site of GW2580, are able to further stabilize the inhibitor-bound state. Using the structural information revealed by these studies, we were able to apply a fragment-linking strategy on one of the promising fragments to suggest
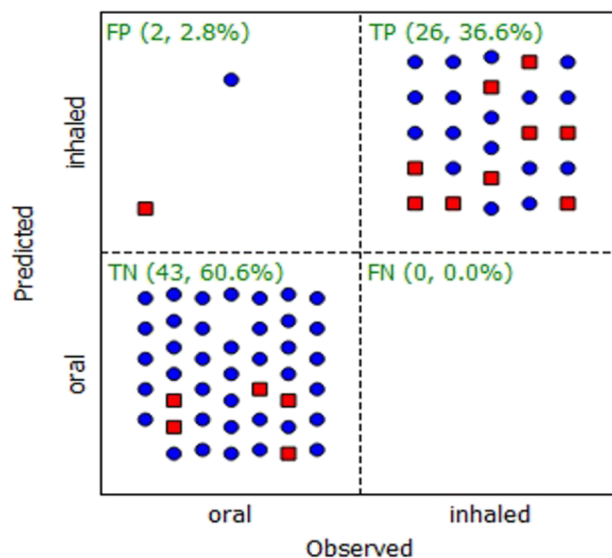
Figure 7. Model Performance matrix. The plot for the 11x1 ANNE classification model includes a graphical two-way truth table, with observed positives (i.e., inhaled route of administration) in the right-hand cells and observed negatives ("oral") in the left-hand cells. Predicted negatives, on the other hand, are in the upper cells and predicted positives are in the lower cells, which puts false negatives in the lower right-hand quadrant. The number and fraction of each class, false negatives (FN), true positives (TP), true negatives (TN), and false positives (FP), are indicated in the top left corner of the respective quadrants. Training pool points are colored blue, whereas test set points are highlighted in red.

several potential next-generation compounds with high predicted binding affinity. We have predicted inhalability of these linked compounds by generating an ANN model, based on the information of currently marketed drugs. This work can contribute to the design and further evaluation of a new class of inhalable asthma therapeutics.

ASSOCIATED CONTENT

Ⓢ Supporting Information

The Supporting Information is available free of charge at https://pubs.acs.org/doi/10.1021/acsomega.3c00803.

ANN architecture; model performance grid of the ANNE models; results by the ICMPocketFinder method; structures of GW2580 linked fragments; 2D ligand interaction plot for GW2580 and protein-ligand RMSD analysis; ICM docked conformations of compounds 2a to 2j; ICM docked conformations of compounds 2k to 2p; HPLC trace for the fragment 7152565; HPLC trace for the fragment 9279194; HPLC trace for the fragment 9208017; details of 71 compounds used for QSPR modeling; list of descriptors generated by AM,[31] used for building the model with the best statistical performance (PDF)

AUTHOR INFORMATION

Corresponding Authors

Michael E. Johnson − *Center for Biomolecular Sciences and Department of Pharmaceutical Sciences, University of Illinois at Chicago, Chicago, Illinois 60607, United States;* orcid.org/0000-0002-8246-4081; Phone: 312-996-9114; Email: mjohnson@uic.edu

Hyun Lee − *Center for Biomolecular Sciences and Department of Pharmaceutical Sciences, University of Illinois at Chicago, Chicago, Illinois 60607, United States; Biophysics Core at Research Resource Center, University of Illinois at Chicago, Chicago, Illinois 60607, United States;* orcid.org/0000-0003-2570-8120; Phone: 312-355-5292; Email: danielhl@uic.edu

Authors

Tasneem M. Vaid − *Center for Biomolecular Sciences and Department of Pharmaceutical Sciences, University of Illinois at Chicago, Chicago, Illinois 60607, United States;* orcid.org/0000-0001-9825-9026

Robel Demissie − *Biophysics Core at Research Resource Center, University of Illinois at Chicago, Chicago, Illinois 60607, United States*

Youngjin Kwon − *Biophysics Core at Research Resource Center, University of Illinois at Chicago, Chicago, Illinois 60607, United States*

Thao Tran − *Center for Biomolecular Sciences and Department of Pharmaceutical Sciences, University of Illinois at Chicago, Chicago, Illinois 60607, United States; Biophysics Core at Research Resource Center, University of Illinois at Chicago, Chicago, Illinois 60607, United States*

Hyung-Geun Moon − *Division of Pulmonary, Critical Care, Sleep and Allergy, Department of Medicine, University of Illinois at Chicago, Chicago, Illinois 60612, United States*

José A. Villegas − *Center for Biomolecular Sciences and Department of Pharmaceutical Sciences, University of Illinois at Chicago, Chicago, Illinois 60607, United States;* orcid.org/0000-0002-4488-347X

Gye Young Park − *Division of Pulmonary, Critical Care, Sleep and Allergy, Department of Medicine, University of Illinois at Chicago, Chicago, Illinois 60612, United States*

Complete contact information is available at:
https://pubs.acs.org/10.1021/acsomega.3c00803

Author Contributions

The manuscript was initially written by T.M.V. and H.L., followed by editions from M.E.J., J.A.V., R.D., H.-G.M., G.Y.P., and H.L. SPR screening, K_D determination, and kinase inhibition (IC_{50}) assays were performed by R.D., Y.K., and T.T. The computational calculations and QSPR modeling were performed by T.M.V. All authors have given approval to the final version of the manuscript.

Notes

The authors declare no competing financial interest.

ACKNOWLEDGMENTS

ABBREVIATIONS

CSF1R, colony stimulating factor-1 receptor; CSF1, colony stimulating factor-1; DC, dendritic cell; SPR, surface plasmon resonance; IC_{50}, half-maximal inhibitory concentration; GAFF, general AMBER force field; PME, particle mesh Ewald; MM/GBSA, molecular mechanics generalized Born surface area; QSPR, quantitative structure−property relationships; AM, ADMET modeler; AP, ADMET predictor; ANN, artificial neural network; ANNE, artificial neural network ensemble; TLA, truncated linear analysis; MCC, Matthews correlation coefficient; FFT, fast Fourier transform; FN, false negatives; TP, true positives; TN, true negatives; FP, false positives

REFERENCES

(1) Peters-Golden, M.; Swern, A.; Bird, S. S.; Hustad, C. M.; Grant, E.; Edelman, J. M. Influence of Body Mass Index on the Response to Asthma Controller Agents. *Eur. Respir. J.* **2006**, *27*, 495−503.

(2) Boulet, L.-P.; Franssen, E. Influence of Obesity on Response to Fluticasone with or without Salmeterol in Moderate Asthma. *Respir. Med.* **2007**, *101*, 2240−2247.

(3) Edris, A.; De Feyter, S.; Maes, T.; Joos, G.; Lahousse, L. Monoclonal Antibodies in Type 2 Asthma: A Systematic Review and Network Meta-Analysis. *Respir. Res.* **2019**, *20*, 179.

(4) Gutowska, M. W. *Comparative Evolutionary and Structural Analysis of the Avian and Mammalian CSF1R Systems*. Ph.D.; University of Edinburgh, 2015. http://hdl.handle.net/1842/15852 (accessed 2021-11-12).

(5) Stanley, E. R.; Chitu, V. CSF-1 Receptor Signaling in Myeloid Cells. *Cold Spring Harbor Perspect. Biol.* **2014**, *6*, No. a021857.

(6) Moon, H.-G.; Kim, S.-J.; Lee, M. K.; Kang, H.; Choi, H. S.; Harijith, A.; Ren, J.; Natarajan, V.; Christman, J. W.; Ackerman, S. J.; Park, G. Y. Colony-Stimulating Factor 1 and Its Receptor Are New Potential Therapeutic Targets for Allergic Asthma. *Allergy* **2020**, *75*, 357−369.

(7) *ClinicalTrials.gov*. https://clinicaltrials.gov/ (accessed 2021-10-26).

(8) Conway, J. G.; Pink, H.; Bergquist, M. L.; Han, B.; Depee, S.; Tadepalli, S.; Lin, P.; Crumrine, R. C.; Binz, J.; Clark, R. L.; Selph, J. L.; Stimpson, S. A.; Hutchins, J. T.; Chamberlain, S. D.; Brodie, T. A. Effects of the CFMS Kinase Inhibitor 5-(3-Methoxy-4-((4-Methoxybenzyl)Oxy)Benzyl)Pyrimidine-2,4-Diamine (GW2580) in Normal and Arthritic Rats. *J. Pharmacol. Exp. Ther.* **2008**, *326*, 41−50.

(9) Shewchuk, L.; Hassell, A.; Holmes, W.; Veal, J.; Emmerson, H.; Musso, D.; Chamberlain, S.; Peckham, G. Crystal Structure of Liganded CFMS Kinase Domain. US20040002145A1, January 1, 2004.

(10) Moon, H.-G.; Kim, S.-J.; Jeong, J. J.; Han, S.-S.; Jarjour, N. N.; Lee, H.; Abboud-Werner, S. L.; Chung, S.; Choi, H. S.; Natarajan, V.; Ackerman, S. J.; Christman, J. W.; Park, G. Y. Airway Epithelial Cell-Derived Colony Stimulating Factor-1 Promotes Allergen Sensitization. *Immunity* **2018**, *49*, 275−287.e5.

(11) Conway, J. G.; McDonald, B.; Parham, J.; Keith, B.; Rusnak, D. W.; Shaw, E.; Jansen, M.; Lin, P.; Payne, A.; Crosby, R. M.; Johnson, J. H.; Frick, L.; Lin, M.-H. J.; Depee, S.; Tadepalli, S.; Votta, B.; James, I.; Fuller, K.; Chambers, T. J.; Kull, F. C.; Chamberlain, S. D.; Hutchins, J. T. Inhibition of Colony-Stimulating-Factor-1 Signaling in Vivo with the Orally Bioavailable CFMS Kinase Inhibitor GW2580. *Proc. Natl. Acad. Sci. U. S. A.* **2005**, *102*, 16078−16083.

(12) Swierczak, A.; Cook, A. D.; Lenzo, J. C.; Restall, C. M.; Doherty, J. P.; Anderson, R. L.; Hamilton, J. A. The Promotion of Breast Cancer Metastasis Caused by Inhibition of CSF-1R/CSF-1 Signaling Is Blocked by Targeting the G-CSF Receptor. *Cancer Immunol. Res.* **2014**, *2*, 765−776.

(13) Leblond, A.-L.; Klinkert, K.; Martin, K.; Turner, E. C.; Kumar, A. H.; Browne, T.; Caplice, N. M. Systemic and Cardiac Depletion of M2 Macrophage through CSF-1R Signaling Inhibition Alters Cardiac Function Post Myocardial Infarction. *PLoS One* **2015**, *10*, No. e0137515.

(14) Adelusi, T. I.; Oyedele, A.-Q. K.; Boyenle, I. D.; Ogunlana, A. T.; Adeyemi, R. O.; Ukachi, C. D.; Idris, M. O.; Olaoba, O. T.; Adedotun, I. O.; Kolawole, O. E.; Xiaoxing, Y.; Abdul-Hammed, M. Molecular Modeling in Drug Discovery. *Inform. Med. Unlocked* **2022**, *29*, No. 100880.

(15) Vaid, T. M.; Chalmers, D. K.; Scott, D. J.; Gooley, P. R. INPHARMA-Based Determination of Ligand Binding Modes at A1-Adrenergic Receptors Explains the Molecular Basis of Subtype Selectivity. *Chemistry* **2020**, *26*, 11796−11805.

(16) Ren, J.; Vaid, T. M.; Lee, H.; Ojeda, I.; Johnson, M. E. Evaluation of Interactions between the Hepatitis C Virus NS3/4A and Sulfonamidobenzamide Based Molecules Using Molecular Docking, Molecular Dynamics Simulations and Binding Free Energy Calculations. *J. Comput.-Aided Mol. Des.* **2023**, *37*, 53−65.

(17) Alshehri, A. S.; You, F. Machine Learning for Multiscale Modeling in Computational Molecular Design. *Curr. Opin. Chem. Eng.* **2022**, *36*, No. 100752.

(18) Ritchie, T. J.; Luscombe, C. N.; Macdonald, S. J. F. Analysis of the Calculated Physicochemical Properties of Respiratory Drugs: Can We Design for Inhaled Drugs Yet? *J. Chem. Inf. Model.* **2009**, *49*, 1025−1032.

(19) Strong, P.; Ito, K.; Murray, J.; Rapeport, G. Current Approaches to the Discovery of Novel Inhaled Medicines. *Drug Discov. Today* **2018**, *23*, 1705−1717.

(20) Tronde, A.; Nordén, B.; Marchner, H.; Wendel, A.-K.; Lennernäs, H.; Bengtsson, U. H. Pulmonary Absorption Rate and Bioavailability of Drugs in Vivo in Rats: Structure-Absorption Relationships and Physicochemical Profiling of Inhaled Drugs. *J. Pharm. Sci.* **2003**, *92*, 1216−1233.

(21) Lee, H.; Cao, S.; Hevener, K. E.; Truong, L.; Gatuz, J. L.; Patel, K.; Ghosh, A. K.; Johnson, M. E. Synergistic Inhibitor Binding to the Papain-Like Protease of Human SARS Coronavirus: Mechanistic and Inhibitor Design Implications. *ChemMedChem* **2013**, *8*, 1361−1372.

(22) Lee, H.; Ren, J.; Pesavento, R. P.; Ojeda, I.; Rice, A. J.; Lv, H.; Kwon, Y.; Johnson, M. E. Identification and Design of Novel Small Molecule Inhibitors against MERS-CoV Papain-like Protease via High-Throughput Screening and Molecular Modeling. *Bioorg. Med. Chem.* **2019**, *27*, 1981−1989.

(23) *Zenobia Fragment Library 1*. zenfragments-copy. https://www.zenobiafragments.com/library-1-c1r08 (accessed 2023-03-20).

(24) *ChemBridge Fragment library*. ChemBridge. https://chembridge.com/screening-compounds/fragments/.

(25) Irwin, J. J.; Shoichet, B. K. ZINC − A Free Database of Commercially Available Compounds for Virtual Screening. *J. Chem. Inf. Model.* **2005**, *45*, 177−182.

(26) Ngan, C. H.; Bohnuud, T.; Mottarella, S. E.; Beglov, D.; Villar, E. A.; Hall, D. R.; Kozakov, D.; Vajda, S. FTMAP: Extended Protein Mapping with User-Selected Probe Molecules. *Nucleic Acids Res.* **2012**, *40*, W271−W275.

(27) An, J.; Totrov, M.; Abagyan, R. Pocketome via Comprehensive Identification and Classification of Ligand Binding Envelopes. *Mol. Cell. Proteomics* **2005**, *4*, 752−761.

(28) Abagyan, R.; Kufareva, I. The Flexible Pocketome Engine for Structural Chemogenomics. *Methods Mol. Biol.* **2009**, *575*, 249−279.

(29) Allen, W. J.; Fochtman, B. C.; Balius, T. E.; Rizzo, R. C. Customizable de Novo Design Strategies for DOCK: Application to HIVgp41 and Other Therapeutic Targets. *J. Comput. Chem.* **2017**, *38*, 2641−2663.

(30) Clark, R. D.; Liang, W.; Lee, A. C.; Lawless, M. S.; Fraczkiewicz, R.; Waldman, M. Using Beta Binomials to Estimate Classification Uncertainty for Ensemble Models. *J Cheminform.* **2014**, *6*, 34.

(31) Simulations Plus. *ADMET property prediction and QSAR model-building application*; Simulations Plus, Inc., 42505 10th Street West, Lancaster, 93534−7059, CA, USA. https://www.simulations-plus.com/software/admetpredictor/.